

HisTrackMap: Global Vectorized High-Definition Map Construction via History Map Tracking

Jing Yang^{* †}
Tongji University

Sen Yang^{*}
Baidu Inc.

Xiao Tan
Baidu Inc.

Hanli Wang[‡]
Tongji University

Abstract

As an essential component of autonomous driving systems, high-definition (HD) maps provide rich and precise environmental information for auto-driving scenarios; however, existing methods, which primarily rely on query-based detection frameworks to directly model map elements or implicitly propagate queries over time, often struggle to maintain consistent temporal perception outcomes. These inconsistencies pose significant challenges to the stability and reliability of real-world autonomous driving and map data collection systems. To address this limitation, we propose a novel end-to-end tracking framework for global map construction by temporally tracking map elements' historical trajectories. Firstly, instance-level historical rasterization map representation is designed to explicitly store previous perception results, which can control and maintain different global instances' history information in a fine-grained way. Secondly, we introduce a Map-Trajectory Prior Fusion module within this tracking framework, leveraging historical priors for tracked instances to improve temporal smoothness and continuity. Thirdly, we propose a global perspective metric to evaluate the quality of temporal geometry construction in HD maps, filling the gap in current metrics for assessing global geometric perception results. Substantial experiments on the nuScenes and Argoverse2 datasets demonstrate that the proposed method outperforms state-of-the-art (SOTA) methods in both single-frame and temporal metrics. The project page is available at: <https://yj772881654.github.io/HisTrackMap>.

1. Introduction

High-definition (HD) maps, which include vectorized map elements such as lane dividers, pedestrian crossings, and road boundaries, play a critical role in the navigation and

planning of autonomous driving [1–5]. Traditional map construction methods use the SLAM-based method [6–8] to collect offline map data, followed by extensive post-processing to generate HD maps. However, these methods are constrained by significant limitations, including substantial costs, the absence of real-time processing capabilities, and difficulties in accommodating dynamic environments and road updates.

Recent advancements in Perspective View (PV)-to-Bird's-Eye View (BEV) methods have significantly enhanced vectorized HD map construction such as [9–12]. These approaches leverage the DETR-based detection paradigm [13] to achieve precise HD map generation. To illustrate the differences across various paradigms. Nevertheless, internal prediction instabilities within the model coupled with uncontrollable environmental factors, such as occlusions or low-light conditions, frequently result in temporal perception inconsistencies, posing substantial challenges for real-world autonomous driving scenarios. Latent query embedding is used as a stream memory [14, 15], facilitating the propagation of temporal information within a unified latent memory. Furthermore, MapTracker [16] employs a tracking paradigm that further utilizes query propagation and implicit latent memory to associate instance-level map elements across consecutive frames, enhancing temporal consistency. In such a framework, a Motion MLP proposed in [15] is essential for obtaining the next-frame latent memory considering the pose transformation between consecutive frames. Consequently, it employs a transformation loss to guide the Motion MLP, implicitly ensuring the accuracy of the pose transformation.

It is understood that a substantial amount of historical perception map data generated during vehicle navigation could potentially be leveraged as prior knowledge or utilized to reduce computational overhead in overlapping map regions. However, the current approach of implicit encoding through instance queries remains inadequate for precisely recording or preserving past geometric map information. To fully utilize existing perception results, we propose HisTrackMap, which explicitly maintains instance-

^{*}Equal contribution.

[†]Work done during an internship at Baidu.

[‡]Corresponding authors.

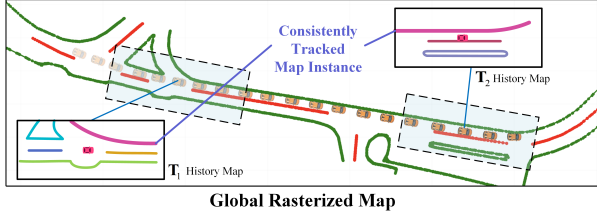


Figure 1. **The global rasterized map with history maps.** Red and green represent divider and boundary categories, respectively. In the history maps, different colors indicate unique tracked map instances. The pink instance is tracked at T_1 , consistently propagating temporal geometric information and providing priors for the corresponding track query at T_2 .

level history maps for corresponding map instances under a tracking paradigm. This approach provides prior information for subsequent navigation perception, ensuring smoother and more continuous HD map construction and enhancing the efficiency and accuracy of temporal information propagation. Fig. 1 illustrates the global rasterized map generated from a continuous navigation sequence, along with details of instance tracking. Furthermore, we propose Map-Trajectory Prior Fusion, which leverages the history map to provide refined prior information for track queries at the subsequent timestamp by integrating position-aligned PV and BEV features. Our HisTrackMap leverages instance-level history maps to establish one-to-one correspondences between track queries and map trajectories, thereby enhancing global geometric consistency and constructing a temporally consistent vectorized HD map.

Although traditional Chamfer Distance mean Average Precision (mAP) metrics are widely used for HD map construction, we argue that single-frame metrics are insufficient for evaluating performance in practical autopilot scenarios and map data collection processes. For example, they fail to maintain global constructed map consistency across sequential frames, which is critical to ensure robust long-term perception, reliable decision-making, and efficient data acquisition. While MapTracker introduced consistency-aware metrics (C-mAP) to penalize inconsistent map elements, they remain indirect methods of evaluation. To address this issue, we propose a global geometric-aware metric (G-mAP), which directly evaluates the global perceptual quality of the entire scene. The proposed HisTrackMap consistently outperforms existing methods, demonstrating the effectiveness of utilizing history maps compared to implicit transformations.

In summary, our main contributions are as follows:

- An end-to-end tracking-enhanced framework, HisTrackMap, for vectorized HD map construction is proposed, which leverages temporal information by maintaining instance-level history maps, reducing redundant computations, and enhancing efficiency.
- The Map-Trajectory Prior Fusion module is designed

to fully utilize the map trajectory information from the history map, combined with instance-level perception features, to provide priors for the corresponding track queries in future frames, thereby optimizing the temporal propagation process.

- A novel benchmark with a global geometric perspective is introduced to address the limitations of existing evaluation methods in practical applications. Our HisTrackMap achieves SOTA results in the popular nuScenes [17] and Argoverse 2 [18] datasets.

2. Related Work

Map Perception with Single Frame. Recently, with advances in PV-to-BEV methods [19–24], the HD map construction has predominantly been formulated as a detection task using surround-view images from vehicle-mounted cameras in a single-frame setting. MapTR [10, 11] proposes a unified approach for map elements, addressing ambiguities and ensuring stable learning. In representing map elements, PivotNet [25] adopts a pivot-based representation, while GeMap [26] models geometric features through Euclidean shapes. MGMapNet [27] leverages multi-granularity representations to model map instances, integrating instance-level and point-level queries.

Map Perception with Priors. Some of the latest methods have also focused on integrating rasterized results and standard (SD) maps to provide priors for HD map construction. SMERF [28] integrates SD maps for online map prediction, with PMapNet [29] enhancing performance by focusing on relevant SD Map skeletons. TopoSD [30] encodes SD map elements into neural representations and instance tokens, using them as priors for lane geometry and topology decoding. Mask2Map [31] uses a two-stage framework, generating a rasterized map via a segmentation network and refining it into a vectorized map with a mask-driven network. HRMapNet [32] leverages historical rasterized maps at the city scale and vehicle localization to improve online vectorized map perception.

Map Perception with Temporal Framework. Temporal information is crucial, particularly in complex scenarios with long distances and occlusions, and has been a consistent focus in 3D object detection [33–36]. StreamMapNet [15] is the first temporal map construction framework. It employs multi-point attention, enabling the construction of large-scale local HD map with high stability. SQD-MapNet [14] introduces the Stream Query Denoising (SQD) strategy for temporal modeling. GlobalMapNet [37] attempts to perform evaluations from a global perspective and proposes Map NMS to obtain a clean global map. MapTracker [16] presents a vector HD-mapping algorithm that formulates the mapping as a tracking task and leverages latent memory to ensure temporally consistent constructions.

3. HisTrackMap

3.1. Overview Architecture

The encoder extracts perception features (BEV feature \mathbf{F}_{bev} and PV feature \mathbf{F}_{pv}) from surrounding-view images to localize spatial structures. The input detection query $\mathbf{Q} \in \mathbb{R}^{N_q \times C}$ is updated through MapDecoder to produce the coordinates $\mathbf{P} \in \mathbb{R}^{N_q \times N_p \times 2}$, categories $\mathbf{C} \in \mathbb{R}^{N_q \times 3}$ (pedestrian, boundary, divider) and scores $\mathbf{S} \in \mathbb{R}^{N_q}$. Here, N_q denotes the number of detected queries, N_p represents the number of points of a map instance, and C is the feature dimension.

After the decoder, the outputted detected queries and propagated track queries are filtered to be positive using a detection threshold τ_{det} and a tracking threshold τ_{track} . These positive N_{track} queries \mathbf{Q}_{track} are propagated to the next frame as new track queries. Queries with confidence below the thresholds are treated as disappeared instances and discarded as negative queries. In summary, map instances will be categorized as newly appeared, consistently tracked, or disappeared, and the corresponding history maps will be initialized, updated with the rasterized map, or removed accordingly. Furthermore, the Map-Trajectory Prior Fusion utilizes the history map to sample corresponding positions on perception features extracted by the encoder, establishing a strong geometric prior for initializing track queries in the new frame and explicitly optimizing the propagation of track queries across temporal sequences.

Section 3.2 introduces the instance-level history maps for maintaining and updating historical map trajectories. Subsequently, Section 3.3 presents the Map-Trajectory Prior Fusion, which provides prior information to enrich track queries. Finally, Section 3.4 proposes the metrics to address the current insufficiencies in evaluating stability and continuity in real-world autonomous driving scenarios.

3.2. Instance-Level History Maps

We first introduce instance-level maps used for storing historical information. The history map is maintained for the tracked instances generated during online prediction to store their trajectory information. During the propagation process, each track query corresponds to a unique map instance and history map, thereby establishing a strong one-to-one relationship.

At the beginning of frame t , \mathcal{M} is a collection of history maps corresponding to a series of track queries, defined as $\mathcal{M}^t = \{\mathbf{M}_i^t \mid i = 1, 2, \dots, N_{track}^{t-1}\}$. Here, each $\mathbf{M}_i^t \in \mathbb{R}^{H \times W}$ indicates the rasterized history map of the i -th instance among the N_{track}^{t-1} instances that have been tracked at the previous frame, where H and W are equal to the height and width of the BEV feature, respectively.

Subsequently, the perception results at timestamp t are used to update the history map. For the j -th instance, if it

is identified as a newly born instance (i.e., no corresponding tracking index is found, and its confidence score \mathbf{S}_j^t exceeds the detect threshold τ_{det}), the rasterization method $\text{Raster}(\cdot)$ [38] is employed to transform the vectorized map representation \mathbf{P}_j^t into a rasterized format. The rasterized result is scaled by \mathbf{S}_j^t to initialize its history map. If the instance has been tracked (i.e., some tracking index is associated, and \mathbf{S}_j^t exceeds the tracking threshold τ_{track}), the corresponding historical map \mathbf{M}_i^{t-1} is retrieved based on its tracking index i . This history map is then temporally decayed using a decay factor λ and updated with the newly rasterized result, yielding the updated history map. After completing the update process, the history map \mathbf{M}_i^t is finalized. At timestamp t , both the total number of tracked instances N_{track}^t and the collection of history maps \mathcal{M}^t are updated accordingly. At the $t + 1$ timestamp, if the confidence score exceeds the threshold τ_{track} , the instance will continue to be tracked. At timestamp $t+1$, \mathcal{M}^t is dynamically aligned with the updated ego position to obtain warped history maps \mathcal{M}_w^{t+1} , thereby enabling initialization for the subsequent timestamp.

Note that, if the prediction confidence of some track query is below the τ_{track} , it indicates that that instance has disappeared or has not been successfully tracked at the current frame. Consequently, it is necessary to remove the corresponding track query and history map \mathbf{M}_r from \mathcal{M}^{t+1} , and the total number of tracked instances N_{track}^{t+1} will be decremented accordingly.

Each map instance follows the process of initialization, tracking, and history map updating to achieve the binding of historical trajectory information with the track query, enabling temporal propagation.

3.3. Map-Trajectory Prior Fusion

As aforementioned, to address the limitations of implicit temporal propagation in capturing detailed feature transformations during motion, the Map-Trajectory Prior Fusion is designed to integrate historical map trajectory information into track queries, enhancing temporal prior utilization and perceptual consistency. The Map-Trajectory Prior Fusion first samples instance features from the history map within the PV and BEV feature spaces. Since the number of instance features varies, padding is applied to align them to a uniform length. These instance-level perception features are then individually integrated into the track queries through cross-attention.

Historical information provides both semantic category and spatial trajectory coordinate data. To enhance the semantic representation of track queries, we define an initial class embedding $\mathbf{CE}_{init} \in \mathbb{R}^{3 \times C}$, which encodes previous track categories into a class embedding $\mathbf{CE} \in \mathbb{R}^{N_{track} \times C}$.

The history map is a fine-grained map with temporal decay. Therefore, we generate the valid pixel mask \mathcal{M}_{val} by

filtering pixels in \mathcal{M} that exceed the map threshold τ_{map} .

Then, we project \mathcal{M}_{val} into the perspective view space using the projection function $\text{Proj}(\cdot)$. In this space, the PV features \mathbf{F}_{pv} are combined with the corresponding positional embedding \mathbf{PE}_{pv} to form enhanced feature representations. Subsequently, the $\text{SampledPV}(\cdot)$ function is applied to sample from these enhanced features, resulting in the final sampled PV features

Similarly, we perform analogous operations in the Bird’s-Eye View space. To ensure that the sampled BEV features $\mathbf{F}_{sampled,bev}$ incorporate positional information, we introduce a sinusoidal position embedding $\mathbf{PE}_{bev} \in \mathbb{R}^{H \times W \times C}$. Then, we utilize \mathcal{M}_{val} to sample BEV feature \mathbf{F}_{bev} through the $\text{SampledBEV}(\cdot)$ function.

Next, the PV and BEV features corresponding to each instance, including the historical map trajectories, have been obtained. The track queries, along with their associated sampled features $\mathbf{F}_{sampled,bev}$ and $\mathbf{F}_{sampled,pv}$, are then utilized within a cross-attention $\text{CA}(\cdot)$ to finalize the initialization of the track queries for the current timestamp.

Finally, we explicitly leverage historical trajectories to provide precise priors for track queries, avoiding redundant auxiliary supervision and inaccurate temporal transformations in implicit propagation. Notably, since the valid pixels for each instance vary, we pad the features and apply a padding mask to ensure that each track query focuses on its corresponding positions.

3.4. Global Geometric HD Mapping Evaluation

Current map construction metrics have the following limitations: (1) Single-frame mAP [10] does not adequately capture the overall quality of a map, as it emphasizes local and instantaneous evaluations while neglecting the assessment of continuity and consistency. (2) consistency-aware C-mAP [16] indirectly addresses consistency but does not explicitly evaluate map completeness. To address these, we propose a global geometric-aware metric (G-mAP) that evaluates construction quality from a global perspective.

First, the vectorized ground truth elements \mathbf{P}_{local}^{gt} from N_{seq} single frames of a sequence segment are projected into a global coordinate system and rasterized to produce a complete global map containing all map instances \mathbf{P}_{global}^{gt} as

$$\mathbf{P}_{global}^{gt} = \text{RasterGlobal}(\{\mathbf{P}_{local}^{gt}\}_{i=1}^{N_{seq}}), \quad (1)$$

where $\text{RasterGlobal}(\cdot)$ denotes the process of transforming local coordinates into the global coordinate system and performing rasterization.

To address truncation issues of polygons (e.g., pedestrians) during vehicle motion, it is more effective to evaluate them using IoU metrics [38]. Thus, we adopt the rasterization-based mAP to evaluate closed pedestrian masks with $AP_{polygon}$. For polyline categories, we use the

Algorithm 1 Global_Instance_Match

Require: Distance cost matrix \mathbf{CM} ,
average confidence scores \mathbf{AS} ,
distance threshold $\tau_{dis} = \{0.25, 0.5, 0.75, 1.0\}$,
valid threshold $\tau_{valid} = 2$

Ensure: True positives \mathbf{TP} , false positives \mathbf{FP}

- 1: $\mathbf{TP} \leftarrow \text{zeros}(\mathbf{CM}.shape[0])$
- 2: $\mathbf{FP} \leftarrow \text{zeros}(\mathbf{CM}.shape[0])$
- 3: $\text{gt_covered} \leftarrow \text{zeros}(\mathbf{CM}.shape[1], \text{dtype} = \text{bool})$
- 4: **for** i in $\text{argsort}(-\mathbf{AS})$ **do**
- 5: **if** $\mathbf{CM}[i].\text{min}() \leq \tau_{dis}$ **then**
- 6: **for** j in $\mathbf{CM}.shape[1]$ **do**
- 7: **if** $\mathbf{CM}[i][j] \leq \tau_{dis}$ and $\text{gt_covered}[j] == \text{False}$ **then**
- 8: $\text{gt_covered}[j] \leftarrow \text{True}$
- 9: $\mathbf{TP}[i] \leftarrow \mathbf{TP}[i] + 1$ // Match multiple ground truth instances
- 10: **end if**
- 11: **end for**
- 12: **else if** $\mathbf{CM}[i].\text{min}() > \tau_{dis} + \tau_{valid}$ **then**
- 13: $\mathbf{FP}[i] \leftarrow 0$ // Invalid FP
- 14: **else if** $\mathbf{CM}[i].\text{min}() \leq \tau_{dis} + \tau_{valid}$ **then**
- 15: $\mathbf{FP}[i] \leftarrow 1$ // Valid FP
- 16: **end if**
- 17: **end for**

Merge function [16] $\text{Merge}(\cdot)$ to combine the tracking results $\mathbf{P}_{local}^{pred}$ from each frame, obtaining a globally complete instance vector $\mathbf{P}_{global}^{pred}$ as

$$\mathbf{P}_{global}^{pred} = \text{Merge}(\{\mathbf{P}_{local}^{pred}\}_{i=1}^{N_{seq}}). \quad (2)$$

To obtain the vector representation of the entire instance, the ground truth mask of the corresponding instance is utilized to extract discrete points via Farthest Point Sampling [39], enabling the fitting of the complete polyline. Subsequently, the $AP_{polyline}$ is calculated using the Chamfer Distance metric [10].

G-mAP leverages the strengths of both rasterized and vectorized representations. It consists of two components: rasterization-based mAP for polygons (e.g., pedestrian) and vectorization-based mAP for polylines (e.g., divider and boundary). By averaging the results across the three categories, G-mAP achieves a comprehensive evaluation from a global geometric perspective.

The `Global_Instance_Match` function is used to obtain false positives (FP) and true positives (TP) under the Chamfer Distance metric. We construct a distance cost matrix $\mathbf{CM} \in \mathbb{R}^{N_{pred} \times N_{gt}}$ using N_{pred} predictions and N_{gt} ground truths, which represents the average distance between the predicted point coordinates and the ground truth for each instance. Additionally, we compute the average

confidence scores $\mathbf{AS} \in \mathbb{R}^{N_{pred}}$ for each instance and define a distance threshold τ_{dis} to evaluate the vectorization-based mAP across different thresholds. It is worth noting that we have optimized the evaluation algorithm due to the unique characteristics of the global perspective. As shown in Algorithm 1, to prevent overlooking shorter instances that have been accurately identified, our algorithm permits predicted instances to correspond to multiple shorter ground truth instances in the global perspective by incrementing the true positive (TP) count. In addition, there are instances in practice that have been perceived but not labelled. To address this issue, we use a validity threshold τ_{valid} to constrain the counting of false positives (FP).

4. Experiments

4.1. Experimental Settings

Dataset. We evaluate HisTrackMap on two popular autonomous driving datasets: nuScenes and Argoverse 2. The nuScenes [17] dataset contains 1,000 scenes, each spanning 20 seconds, with data from six synchronized RGB cameras and detailed pose information. The Argoverse 2 dataset [18] includes 1,000 sequences with high-resolution images from seven ring cameras, two stereo cameras, LiDAR point clouds, and map-aligned 6-DoF pose data. Experiments were conducted on both the old [10] and new [15] dataset splits for comprehensive evaluation.

Metrics. Following previous work [10, 11, 15, 16, 27], we adopt mean Average Precision (mAP) as the primary evaluation metric. Evaluation thresholds are set at 0.5m, 1.0m, and 1.5m. AP_{ped} , AP_{div} , and AP_{bou} represent average precision for pedestrians, dividers, and boundaries, respectively. In addition, we employ consistency-aware metric (C-mAP) [16] and further introduce a novel global geometric-aware augmented metric (G-mAP), as detailed in Sec. 3.4.

Implementation Details. Our framework builds on MapTracker [16], which serves as the primary baseline. We removed the Motion MLP and the auxiliary transformation loss used for its supervision while keeping other loss functions consistent with MapTracker. Training on the nuScenes [17] dataset was conducted on 8 NVIDIA RTX A100 GPUs for 72 epochs across three stages (18, 6, and 48 epochs). Similarly, we trained on the Argoverse2 [18] dataset for 35 epochs (12, 3, and 20 epochs) to align with MapTracker. Additionally, to ensure alignment with methods such as MapTR [10, 27, 32], we evaluated a shorter 24-epoch training configuration on both datasets. To address inaccuracies in the PV projection caused by the dataset’s missing Z-axis coordinates, we introduced a complete MapTrajectory Prior Fusion in Stage 2 to accelerate model convergence. In Stage 3, we exclusively adopted a single BEV Prior to further enhancing model performance. The hy-

perparameters are configured as $N_q = 100$, $N_p = 20$, $C = 512$, $\tau_{det} = 0.4$, $\tau_{track} = 0.5$, $\tau_{map} = 0.5$, $\lambda = 0.95$.

4.2. Comparison with SOTA Method

Comparison on nuScenes. As shown in Table 1, we compare HisTrackMap with state-of-the-art methods. HisTrackMap demonstrates superior performance at 24 epochs, achieving 73.8 mAP, outperforming MapTracker, which achieves 71.9 mAP, by +1.9 mAP. In addition, HisTrackMap achieves 64.7 C-mAP and 48.5 G-mAP, outperforming MapTracker by +1.3 C-mAP and +1.2 G-mAP, respectively. In the 72-epoch experiment, HisTrackMap achieved 76.6 mAP, 68.7 C-mAP, and 50.2 G-mAP respectively. Furthermore, recent methods like Mask2Map and MGMap use single-frame frameworks with limited temporal modeling, while HisTrackMap outperforms them in all metrics. Notably, by removing transformation loss supervision of Motion MLP, HisTrackMap achieves about 20% faster training than MapTracker. During inference, HisTrackMap runs at 10.3 FPS, slightly slower than MapTracker’s 10.9 FPS due to feature sampling overhead, which could be optimized with parallel acceleration in practical applications. In summary, HisTrackMap improves performance and remains practical for real-time autonomous driving applications.

Comparison on Argoverse 2. The results on the Argoverse 2 dataset, as presented in Table 2, further validate the effectiveness of HisTrackMap. In the 24-epoch experiment, HisTrackMap achieves a notable mAP improvement of +8.5 over HRMapNet and +9.4 over MapTRv2. Additionally, HisTrackMap surpasses MapTracker with +1.2 mAP, +3.5 C-mAP, and +0.8 G-mAP at 24 epochs, and +0.9 mAP, +1.2 C-mAP, and +0.6 G-mAP at 35 epochs. Note that due to the different sampling intervals of HisTrackMap and MapTracker on the Argoverse 2 dataset compared to the other methods, we can only evaluate the mAP metrics.

Comparison on non-overlapping datasets. The nuScenes and Argoverse 2 datasets exhibit geographical overlaps [42]. StreamMapNet [14] proposes a non-overlapping dataset split for them. The experimental results are shown in Table 3. Our method surpasses MapTracker, achieving improvements of +1.2 mAP, +0.3 C-mAP, and +0.5 G-mAP on nuScenes, and +1.1 mAP, +1.4 C-mAP, and +0.9 G-mAP on Argoverse 2. We conducted cross-dataset experiments to demonstrate further the superior generalization of HisTrackMap. The encoder and decoder were initialized with weights from nuScenes and Argoverse 2 respectively, and finetuned for 12 epochs on the nuScenes newsplit before testing. HisTrackMap achieved 44.5 mAP, 35.1 C-mAP, and 31.2 G-mAP, demonstrating superior generalization performance over MapTracker.

Method	Epoch	AP_{ped}	AP_{div}	AP_{bou}	mAP	C-mAP	G-mAP	FPS
MapTRv2 [10] [IJCV2024]	24	59.8	62.4	62.4	61.4	41.7	33.9	14.1
StreamMapNet [14] [WACV2024]	24	61.9	66.3	62.1	63.4	38.4	34.3	13.1
HRMapNet [32] [ECCV2024]	24	65.8	67.4	68.5	67.3	49.2	39.7	10.3
MGMap [40] [CVPR2024]	24	61.8	65.0	67.5	64.8	43.5	39.1	13.4
MGMapNet [27] [ICLR2025]	24	64.7	66.1	69.4	66.8	45.4	37.5	11.7
HRMapNet [32] [ECCV2024]	110	72.0	72.9	75.8	73.6	61.4	47.9	10.3
Mask2Map [31] [ECCV2024]	110	73.6	73.1	77.3	74.6	60.3	48.8	9.2
MapTracker [16] [ECCV2024]	72	80.0	74.1	74.1	76.1	69.1	49.4	10.9
HisTrackMap (Ours)	72	79.8	74.5	75.4	76.6	68.7	50.2	10.3

Table 1. Comparison with SOTA methods on the nuScenes validation set. † indicates the version reproduced.

Method	epoch	AP_{ped}	AP_{div}	AP_{bou}	mAP	C-mAP	G-mAP
MapTRv2 [10] [IJCV2024]	24	62.9	72.1	67.1	67.4	–	–
HRMapNet [32] [ECCV2024]	30	65.1	71.4	68.6	68.3	–	–
HIMap [41] [CVPR2024]	24	72.4	72.4	73.2	72.7	–	–
MGMapNet [27] [ICLR2025]	24	71.3	76.0	73.1	73.6	–	–
MapTracker [16] [ECCV2024]	35	76.9	79.9	73.6	76.8	68.3	48.0
HisTrackMap (Ours)	35	78.8	80.1	74.0	77.7	69.5	48.6

Table 2. Comparison with SOTA methods on the Argoverse2 validation set. The ‘–’ symbol indicates that no results are provided.

Dataset	Method	mAP	C-mAP	G-mAP
nuScenes	MapTracker	40.3	32.5	28.0
	HisTrackMap	41.5	32.8	28.5
Argoverse2	MapTracker	70.3	61.3	48.3
	HisTrackMap	71.4	62.7	49.2
Unified nuScenes	MapTracker	43.5	34.0	29.9
	HisTrackMap	44.5	35.1	31.2

Table 3. Comparisons on non-overlapping datasets.

4.3. Quantitative Evaluations

Fig. 2 presents a qualitative comparison between HisTrackMap and other methods on nuScenes dataset. We utilized the integration [16] of per-frame vectorized HD maps into a global vectorized HD map for better visualization. The rectangular regions highlight instances where our proposed model exhibits superior perception performance. The orange markings indicate that HisTrackMap accurately identified the two separate boundaries at the turning, whereas MapTracker failed to distinguish them. The blue markings highlight that HisTrackMap achieved continuous and consistent tracking through a complex intersection, whereas MapTracker lost the polyline. The green markings indicate that HisTrackMap fully detected the boundary, while MapTracker captured only the first half. In this green example, all models detected a divider that was not actually annotated, emphasizing the necessity of optimizing false positive (FP) counting in G-mAP. Furthermore, although single-frame MapTRv2 can partially perceive re-

sults, the integrated results lack sufficient stability and fail to maintain consistent perception. In general, HisTrackMap delivers more accurate and cleaner results, demonstrating superior performance in terms of overall quality and temporal consistency.

4.4. Ablation and Robustness Studies

The proposed Map-Trajectory Prior Fusion consists of three main components: Class Embedding, PV Prior, and BEV Prior. To evaluate the contributions of each component, we conducted an ablation study on the nuScenes dataset. The experiment without Map-Trajectory Prior Fusion is used as the baseline. There are several observations from the results. First, introducing Class Embedding improved mAP by 0.7, demonstrating the effectiveness of semantic category priors. Second, incorporating PV Prior and BEV Prior based on Class Embedding further improves mAP from 72.3 to 72.9 and 73.3, respectively. This reveals that it is beneficial to utilize geometric trajectory information to enhance track queries. Third, with the complete Map-Trajectory Prior Fusion, the model achieved the highest 73.8 mAP, highlighting the significance of history map based trajectory priors in effectively leveraging temporal-spatial information to enhance perception performance.

The update of the history map primarily relies on the vehicle’s motion pose parameters. To evaluate the robustness of HisTrackMap to localization errors, we conducted additional experiments on the nuScenes dataset. Random noise was introduced to the translation and rotation of the extrinsic matrix to disrupt the history map update. The results

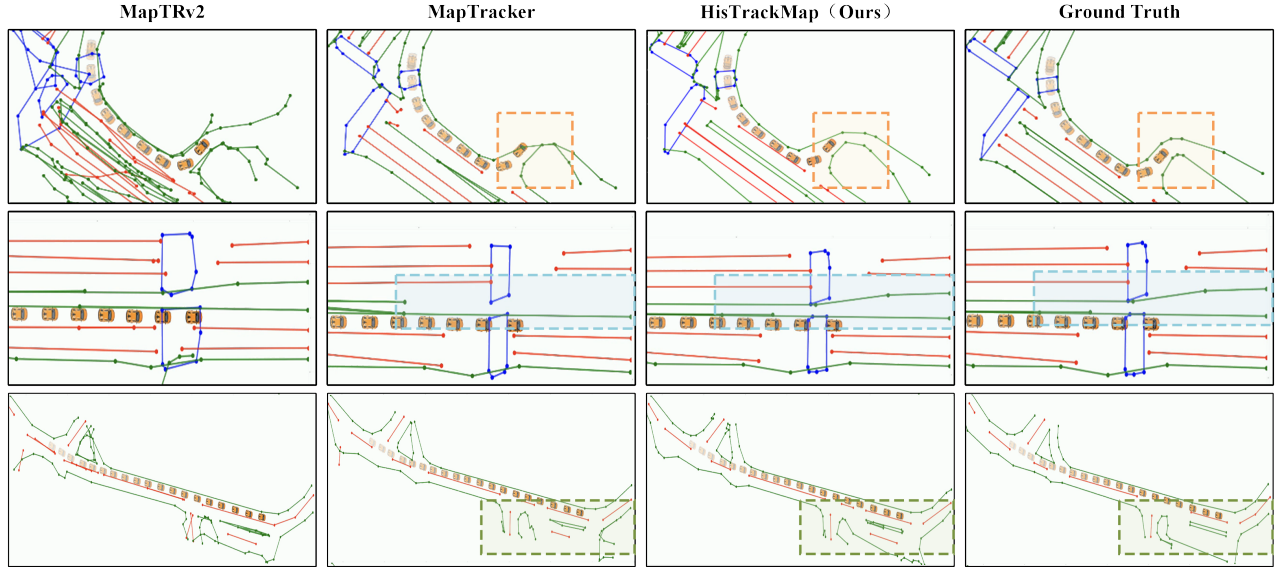


Figure 2. Qualitative visualization on nuScenes val set.

show that the model achieves 73.0 mAP under noise levels of 0.2 m and 0.02 rad and 73.4 mAP under real-world noise levels (0.1 m, 0.01 rad), maintaining a clear advantage. The experimental results continue to outperform most previous single-frame models, demonstrating the practical effectiveness of HisTrackMap.

5. Conclusion

In this work, we introduce a novel method for end-to-end vectorized HD map construction via tracking history maps, enabling more robust and efficient temporal association modeling. Specifically, the history map is systematically constructed and updated based on past perception results, thereby minimizing redundant computations. We introduce the Map-Trajectory Prior Fusion method, which integrates historical map data with current perception features to improve the precision of frame-to-frame transformations. Additionally, we propose a global geometric HD mapping evaluation framework that focuses on assessing overall map construction quality. This evaluation is vital for both autonomous driving systems and map data collection processes. In the future, it is desired to extend the current work by exploring a more robust, reliable, and adaptive perception system considering the existence of vehicle localization errors.

References

- [1] X. Xiong, Y. Liu, T. Yuan, Y. Wang, Y. Wang, and H. Zhao, "Neural map prior for autonomous driving," in *Proceedings of the IEEE/CVF Conference on Computer Vision and Pattern Recognition*, 2023, pp. 17 535–17 544. 1
- [2] Y. Xiao, F. Codevilla, A. Gurram, O. Urfalioglu, and A. M. López, "Multimodal end-to-end autonomous driving," *IEEE Transactions on Intelligent Transportation Systems*, vol. 23, no. 1, pp. 537–547, 2020.
- [3] Z. Xu, Y. Zhang, E. Xie, Z. Zhao, Y. Guo, K.-Y. K. Wong, Z. Li, and H. Zhao, "DriveGPT4: interpretable end-to-end autonomous driving via large language model," *IEEE Robotics and Automation Letters*, 2024.
- [4] A. Prakash, K. Chitta, and A. Geiger, "Multi-modal fusion transformer for end-to-end autonomous driving," in *Proceedings of the IEEE/CVF conference on computer vision and pattern recognition*, 2021, pp. 7077–7087.
- [5] T. Li, H. Wang, X. Li, W. Liao, T. He, and P. Peng, "Generative planning with 3d-vision language pre-training for end-to-end autonomous driving," *arXiv preprint arXiv:2501.08861*, 2025. 1
- [6] T. Shan, B. Englot, D. Meyers, W. Wang, C. Ratti, and D. Rus, "LIO-SAM: tightly-coupled lidar inertial odometry via smoothing and mapping," in *2020 IEEE/RSJ international conference on intelligent robots and systems (IROS)*. IEEE, 2020, pp. 5135–5142. 1
- [7] T. Shan and B. Englot, "LeGO-LOAM: lightweight and ground-optimized lidar odometry and mapping on variable terrain," in *2018 IEEE/RSJ International Conference on Intelligent Robots and Systems (IROS)*. IEEE, 2018, pp. 4758–4765.
- [8] J. Zhang, S. Singh *et al.*, "LOAM: lidar odometry and mapping in real-time." in *Robotics: Science and systems*, vol. 2, no. 9. Berkeley, CA, 2014, pp. 1–9. 1
- [9] Q. Li, Y. Wang, Y. Wang, and H. Zhao, "HDMaNet: an online HD map construction and evaluation framework," in *2022 International Conference on Robotics and Automation (ICRA)*. IEEE, 2022, pp. 4628–4634. 1
- [10] B. Liao, S. Chen, Y. Zhang, B. Jiang, Q. Zhang, W. Liu, C. Huang, and X. Wang, "MapTRv2: an end-to-end framework for online vectorized HD map construction," *arXiv preprint arXiv:2308.05736*, 2023. 2, 4, 5, 6

- [11] B. Liao, S. Chen, X. Wang, T. Cheng, Q. Zhang, W. Liu, and C. Huang, “MapTR: structured modeling and learning for online vectorized HD map construction,” *arXiv preprint arXiv:2208.14437*, 2022. 2, 5
- [12] A. Hu, Z. Murez, N. Mohan, S. Dudas, J. Hawke, V. Badrinarayanan, R. Cipolla, and A. Kendall, “FIERY: future instance prediction in bird’s-eye view from surround monocular cameras,” in *Proceedings of the IEEE/CVF International Conference on Computer Vision*, 2021, pp. 15 273–15 282. 1
- [13] N. Carion, F. Massa, G. Synnaeve, N. Usunier, A. Kirillov, and S. Zagoruyko, “End-to-end object detection with transformers,” in *European conference on computer vision*. Springer, 2020, pp. 213–229. 1
- [14] S. Wang, F. Jia, Y. Liu, Y. Zhao, Z. Chen, T. Wang, C. Zhang, X. Zhang, and F. Zhao, “Stream query denoising for vectorized HD map construction,” *arXiv preprint arXiv:2401.09112*, 2024. 1, 2, 5, 6
- [15] T. Yuan, Y. Liu, Y. Wang, Y. Wang, and H. Zhao, “StreamMapNet: streaming mapping network for vectorized online HD map construction,” in *Proceedings of the IEEE/CVF Winter Conference on Applications of Computer Vision*, 2024, pp. 7356–7365. 1, 2, 5
- [16] J. Chen, Y. Wu, J. Tan, H. Ma, and Y. Furukawa, “MapTracker: tracking with strided memory fusion for consistent vector HD mapping,” in *European Conference on Computer Vision*. Springer, 2025, pp. 90–107. 1, 2, 4, 5, 6
- [17] H. Caesar, V. Bankiti, A. H. Lang, S. Vora, V. E. Liong, Q. Xu, A. Krishnan, Y. Pan, G. Baldan, and O. Beijbom, “nuScenes: a multimodal dataset for autonomous driving,” in *Proceedings of the IEEE/CVF conference on computer vision and pattern recognition*, 2020, pp. 11 621–11 631. 2, 5
- [18] B. Wilson, W. Qi, T. Agarwal, J. Lambert, J. Singh, S. Khadelwal, B. Pan, R. Kumar, A. Hartnett, J. K. Pontes *et al.*, “Argoverse 2: next generation datasets for self-driving perception and forecasting,” *arXiv preprint arXiv:2301.00493*, 2023. 2, 5
- [19] C. Yang, Y. Chen, H. Tian, C. Tao, X. Zhu, Z. Zhang, G. Huang, H. Li, Y. Qiao, L. Lu *et al.*, “BEVFormer v2: adapting modern image backbones to bird’s-eye-view recognition via perspective supervision,” in *Proceedings of the IEEE/CVF Conference on Computer Vision and Pattern Recognition*, 2023, pp. 17 830–17 839. 2
- [20] Z. Li, W. Wang, H. Li, E. Xie, C. Sima, T. Lu, Q. Yu, and J. Dai, “BEVFormer: learning bird’s-eye-view representation from lidar-camera via spatiotemporal transformers,” *IEEE Transactions on Pattern Analysis and Machine Intelligence*, 2024.
- [21] J. Philion and S. Fidler, “Lift, splat, shoot: encoding images from arbitrary camera rigs by implicitly unprojecting to 3D,” in *Computer Vision—ECCV 2020: 16th European Conference, Glasgow, UK, August 23–28, 2020, Proceedings, Part XIV 16*. Springer, 2020, pp. 194–210.
- [22] Y. Liu, T. Wang, X. Zhang, and J. Sun, “PETR: position embedding transformation for multi-view 3D object detection,” in *European conference on computer vision*. Springer, 2022, pp. 531–548.
- [23] Y. Liu, J. Yan, F. Jia, S. Li, A. Gao, T. Wang, and X. Zhang, “PETR v2: a unified framework for 3D perception from multi-camera images,” in *Proceedings of the IEEE/CVF International Conference on Computer Vision*, 2023, pp. 3262–3272.
- [24] Y. Liu, T. Yuan, Y. Wang, Y. Wang, and H. Zhao, “VectorMapNet: end-to-end vectorized HD map learning,” in *International Conference on Machine Learning*. PMLR, 2023, pp. 22 352–22 369. 2
- [25] W. Ding, L. Qiao, X. Qiu, and C. Zhang, “PivotNet: vectorized pivot learning for end-to-end HD map construction,” in *Proceedings of the IEEE/CVF International Conference on Computer Vision*, 2023, pp. 3672–3682. 2
- [26] Z. Zhang, Y. Zhang, X. Ding, F. Jin, and X. Yue, “Online vectorized HD map construction using geometry,” in *European Conference on Computer Vision*. Springer, 2025, pp. 73–90. 2
- [27] J. Yang, M. Jiang, S. Yang, X. Tan, Y. Li, E. Ding, H. Wang, and J. Wang, “MGMapNet: multi-granularity representation learning for end-to-end vectorized HD map construction,” *arXiv preprint arXiv:2410.07733*, 2024. 2, 5, 6
- [28] K. Z. Luo, X. Weng, Y. Wang, S. Wu, J. Li, K. Q. Weinberger, Y. Wang, and M. Pavone, “Augmenting lane perception and topology understanding with standard definition navigation maps,” in *2024 IEEE International Conference on Robotics and Automation (ICRA)*. IEEE, 2024, pp. 4029–4035. 2
- [29] Z. Jiang, Z. Zhu, P. Li, H.-a. Gao, T. Yuan, Y. Shi, H. Zhao, and H. Zhao, “P-MapNet: far-seeing map generator enhanced by both SDMap and HDMap priors,” *arXiv preprint arXiv:2403.10521*, 2024. 2
- [30] S. Yang, M. Jiang, Z. Fan, X. Xie, X. Tan, Y. Li, E. Ding, L. Wang, and J. Wang, “TopoSD: topology-enhanced lane segment perception with SDMap prior,” *arXiv preprint arXiv:2411.14751*, 2024. 2
- [31] S. Choi, J. Kim, H. Shin, and J. W. Choi, “Mask2Map: vectorized HD map construction using bird’s eye view segmentation masks,” *arXiv preprint arXiv:2407.13517*, vol. 2, 2024. 2, 6
- [32] X. Zhang, G. Liu, Z. Liu, N. Xu, Y. Liu, and J. Zhao, “Enhancing vectorized map perception with historical rasterized maps,” in *European Conference on Computer Vision*. Springer, 2025, pp. 422–439. 2, 5, 6
- [33] J. Huang and G. Huang, “BEVDet4D: exploit temporal cues in multi-camera 3D object detection,” *arXiv preprint arXiv:2203.17054*, 2022. 2
- [34] S. Wang, Y. Liu, T. Wang, Y. Li, and X. Zhang, “Exploring object-centric temporal modeling for efficient multi-view 3D object detection,” in *Proceedings of the IEEE/CVF international conference on computer vision*, 2023, pp. 3621–3631.
- [35] C. Han, J. Yang, J. Sun, Z. Ge, R. Dong, H. Zhou, W. Mao, Y. Peng, and X. Zhang, “Exploring recurrent long-term temporal fusion for multi-view 3D perception,” *IEEE Robotics and Automation Letters*, 2024.
- [36] X. Lin, T. Lin, Z. Pei, L. Huang, and Z. Su, “Sparse4D v2: recurrent temporal fusion with sparse model,” *arXiv preprint arXiv:2305.14018*, 2023. 2

- [37] A. Shi, Y. Cai, X. Chen, J. Pu, Z. Fu, and H. Lu, “GlobalMapNet: An online framework for vectorized global hd map construction,” *arXiv preprint arXiv:2409.10063*, 2024. [2](#)
- [38] G. Zhang, J. Lin, S. Wu, Z. Luo, Y. Xue, S. Lu, Z. Wang *et al.*, “Online map vectorization for autonomous driving: a rasterization perspective,” *Advances in Neural Information Processing Systems*, vol. 36, 2024. [3](#), [4](#)
- [39] C. R. Qi, L. Yi, H. Su, and L. J. Guibas, “PointNet++: deep hierarchical feature learning on point sets in a metric space,” *Advances in neural information processing systems*, vol. 30, 2017. [4](#)
- [40] X. Liu, S. Wang, W. Li, R. Yang, J. Chen, and J. Zhu, “MGMap: mask-guided learning for online vectorized HD map construction,” in *Proceedings of the IEEE/CVF Conference on Computer Vision and Pattern Recognition*, 2024, pp. 14 812–14 821. [6](#)
- [41] Y. Zhou, H. Zhang, J. Yu, Y. Yang, S. Jung, S.-I. Park, and B. Yoo, “HIMap: hybrid representation learning for end-to-end vectorized HD map construction,” in *Proceedings of the IEEE/CVF Conference on Computer Vision and Pattern Recognition*, 2024, pp. 15 396–15 406. [6](#)
- [42] A. Lilja, J. Fu, E. Stenborg, and L. Hammarstrand, “Localization is all you evaluate: data leakage in online mapping datasets and how to fix it,” in *Proceedings of the IEEE/CVF Conference on Computer Vision and Pattern Recognition*, 2024, pp. 22 150–22 159. [5](#)